Inelastic X-ray scattering from electronic excitations

Introduction
Some theoretical background
Experimental aspects

X-ray Raman scattering
Resonant inelastic X-ray scattering

Fluorescence spectroscopy (under high pressure)

(Trieste, 16. May 2006)

Schematic inelastic x-ray spectrum

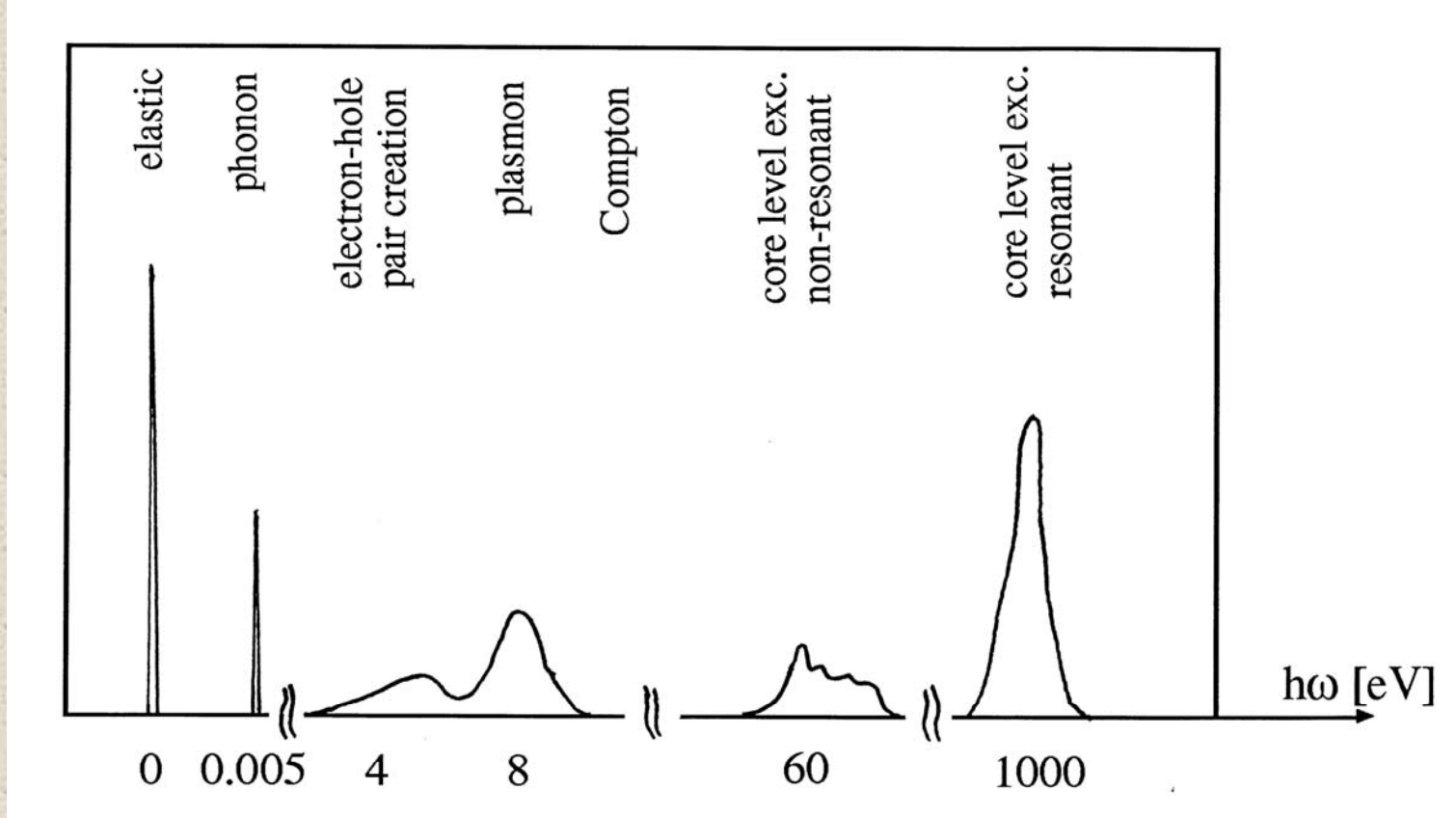

Energy Transfer [eV]

Why IXS from electronic excitations ?

Complementary
to other core- and valence level spectroscopies

- (Soft) x-ray absorption spectroscopy (dichroism)
- Photoemission
- Electron energy loss

- element, valence, orbital and spin-selectivity
- bulk sensitivity
- extreme conditions (high pressure)

Photon-electron interaction

1) Scattering of a photon (**A·A** in 1. Order)

- non-resonant

2) Scattering of a photon (**p·A** in 2. Order)

- resonant scattering
- absorption followed by emission

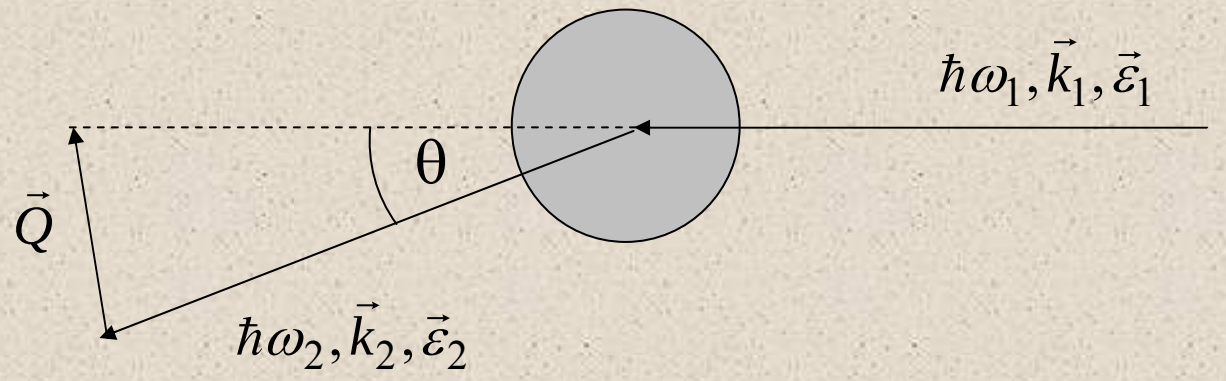

Experimental IXS set-up

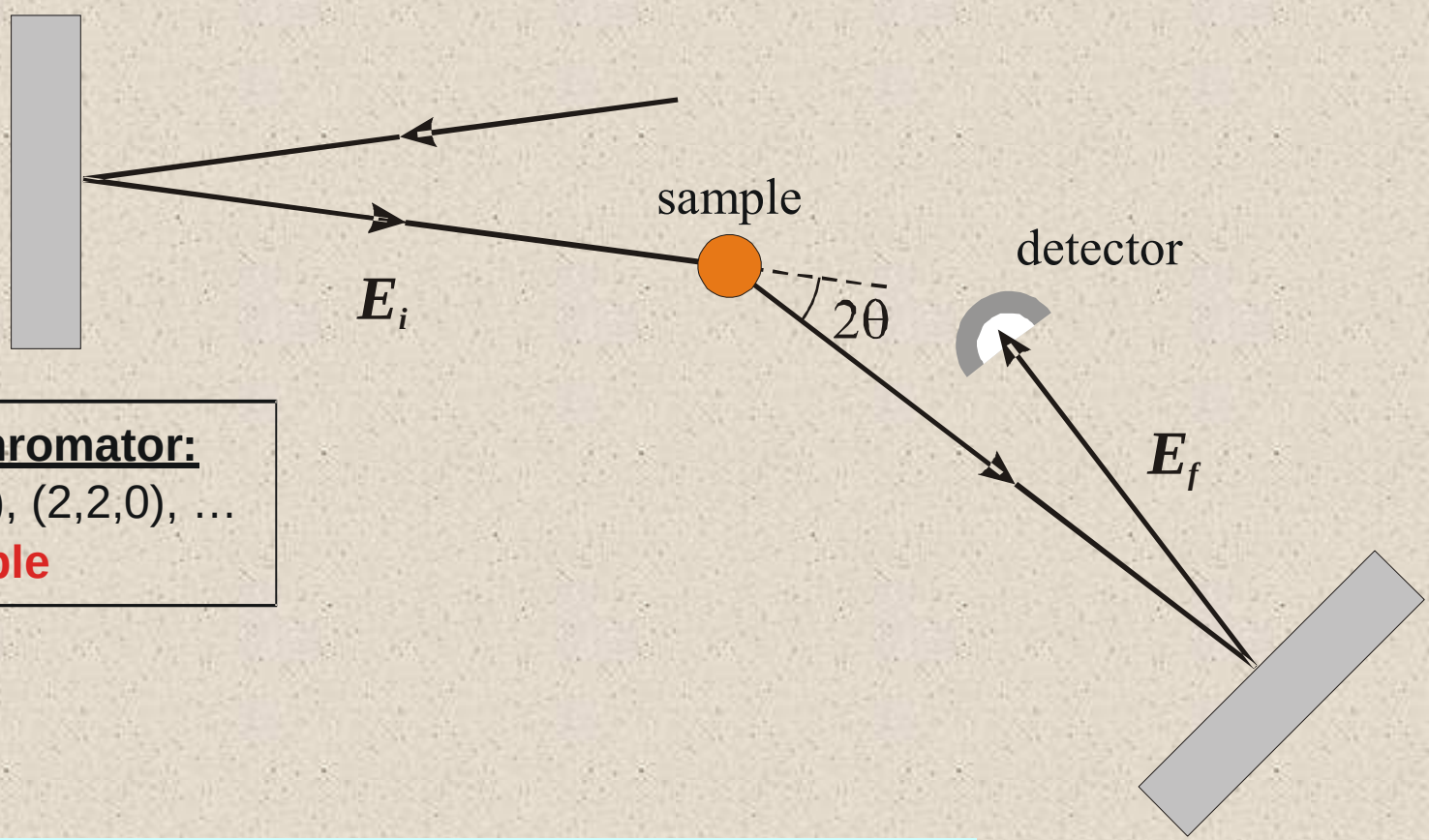

Monochromator:
Si(1,1,1), (2,2,0), …
λ_1 **tunable**

Tunability via angle, and not temperature.

Analyser:
Si(h,k,l)
λ_1 **tunable**

Experimental Setup (ID16 at ESRF)

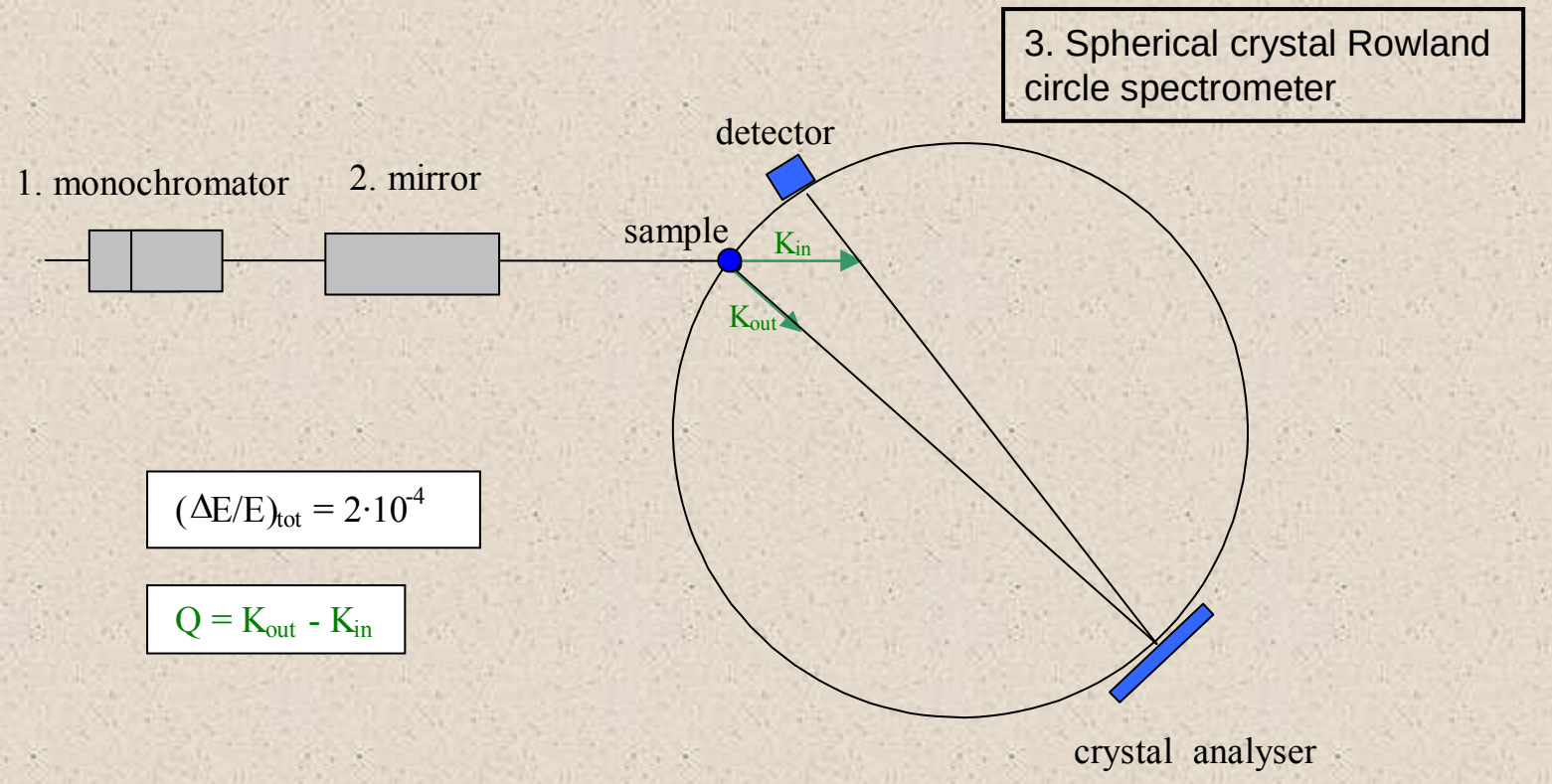

1. Si (111) scanning double crystal monochromator.
2. Toroidal mirror to produce small focal spot at sample.
3. Crystal spectrometer to energy analyze the scattered photons:
   1m spherical crystal, typically Si (440) to Si (555) at Bragg angles 65º - 90º.

Scanning modes

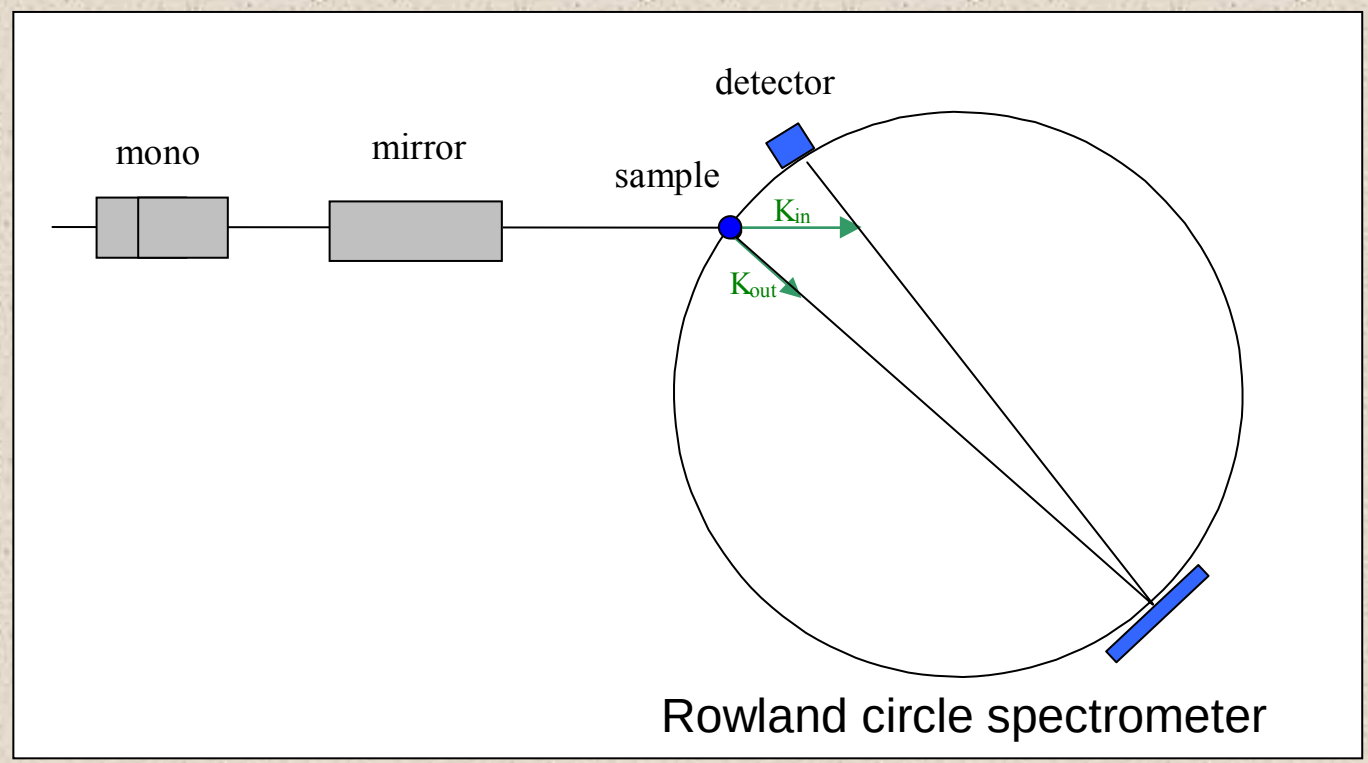

1. $h\omega_2$ fixed, scanning $h\omega_1$	non-resonant IXS, RIXS
2. $h\omega_1$ fixed, scanning $h\omega_2$ (rotating crystal and follow with the detector)	RIXS
3. Scanning $h\omega_1$ and $h\omega_2$ (keeping energy transfer constant)	RIXS

X-ray Raman scattering

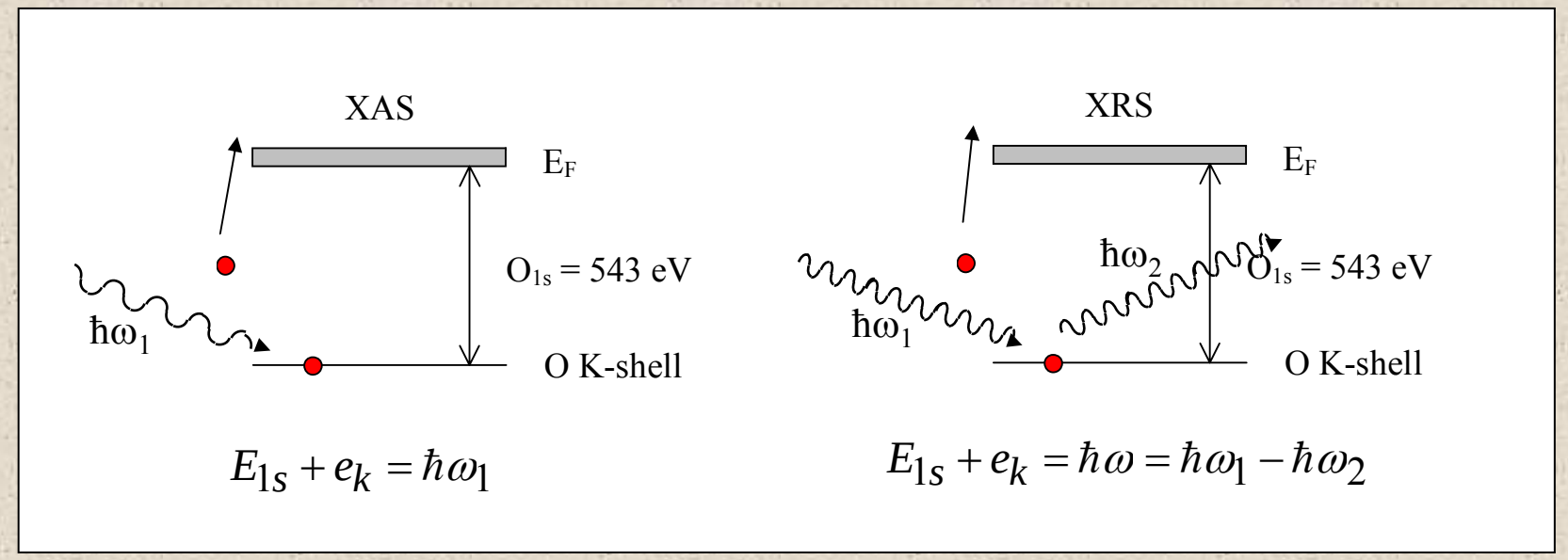

Role of incident photon energy in XAS is played by the energy transfer in XRS

=>

certain freedom in the choice of the incident photon energy

Hard X-rays => Bulk sensitivity; Access to buried layers
High pressure and/or temperature

X-ray absorption cross section (dipolar approximation):

$$\frac{d\sigma}{d\omega_1} = 4\pi^2 \alpha \hbar \omega_1 \sum_F \left| \langle F | \vec{\varepsilon}_1 \cdot \vec{r} | I \rangle \right|^2 \delta(E_F - E_I - \hbar\omega_1)$$

X-ray Raman cross section:

$$\frac{d^2\sigma}{d\omega_2 d\Omega} = r_0^2 \frac{\omega_2}{\omega_1} (\vec{\varepsilon}_1 \cdot \vec{\varepsilon}_2) \sum_F \left| \langle F | \sum_j e^{i\vec{Q}\vec{r}_j} | I \rangle \right|^2 \delta(E_F - E_I - \hbar\omega)$$

Qr << 1: $e^{iQr} \approx 1 + iQr$

Dipolar regime: identical to photon absorption, where **Q** plays the role of the photon polarization vector e_1.

Qr > 1: e^{iQr}

Multipolar regime: monopolar, dipolar and quadrupolar transitions possible.

XRS from the O K-edge in water and ice

D.T. Bowron et al.; Phys. Rev. B 62, R9223 (2000)

Motivation: probe element-specific local atomic structure in disordered systems

Alternative techniques:

- (Isotopic substitution) neutron scattering
- X-ray (anomalous) scattering

- XANES and EXAFS

Complete IXS spectrum

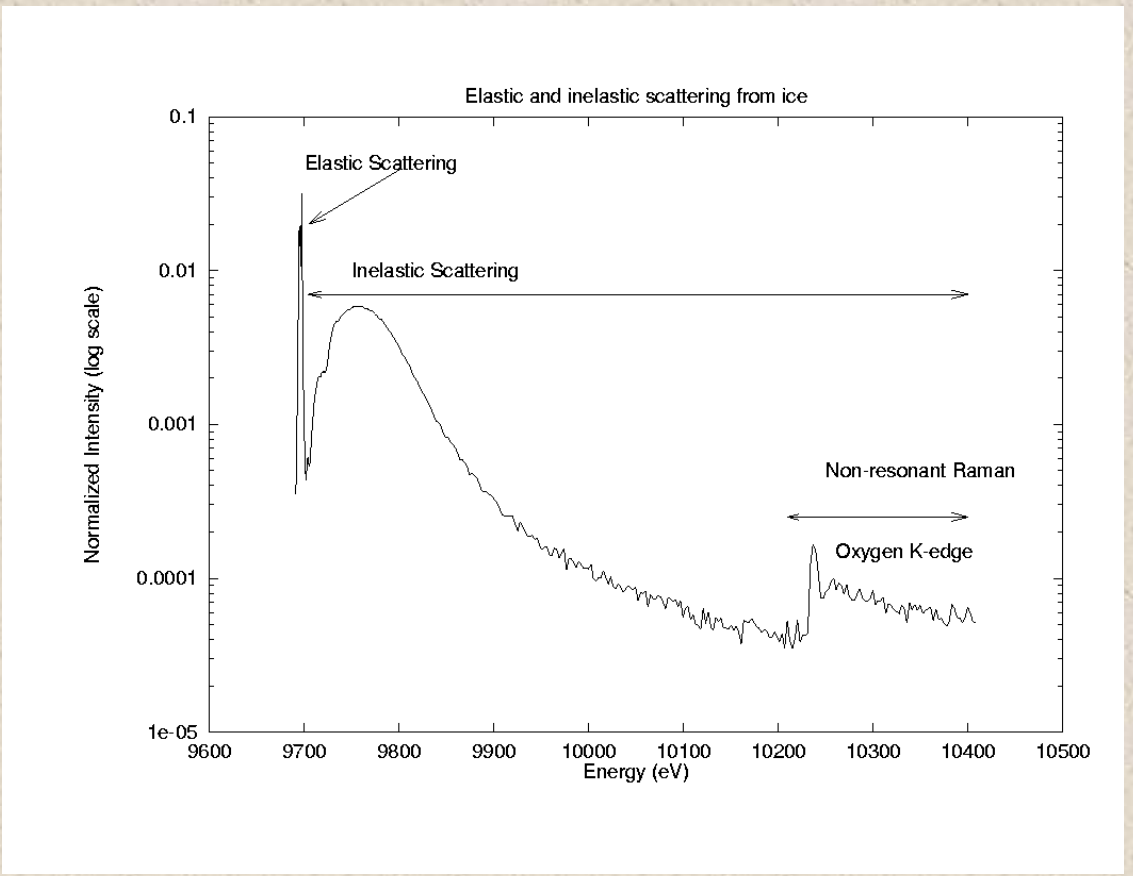

$h\omega_2$ = 9686 eV

ΔE = 2 eV

Q = 4.38 A^{-1} (Qr = 0.29)

k < 7 A^{-1}

XRS XANES- and EXAFS spectrum of O K-edge

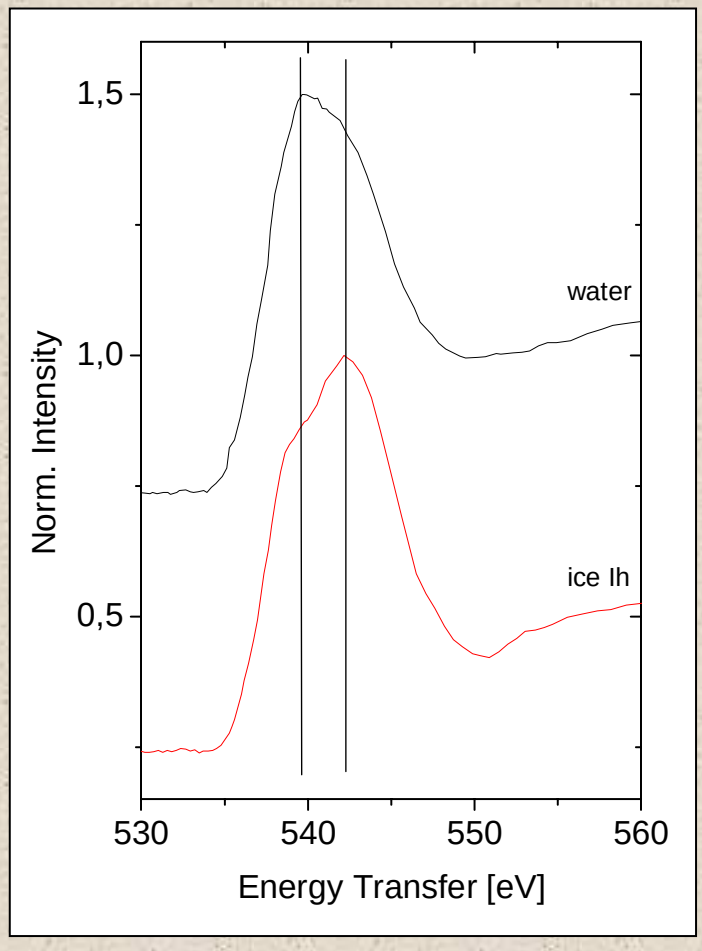

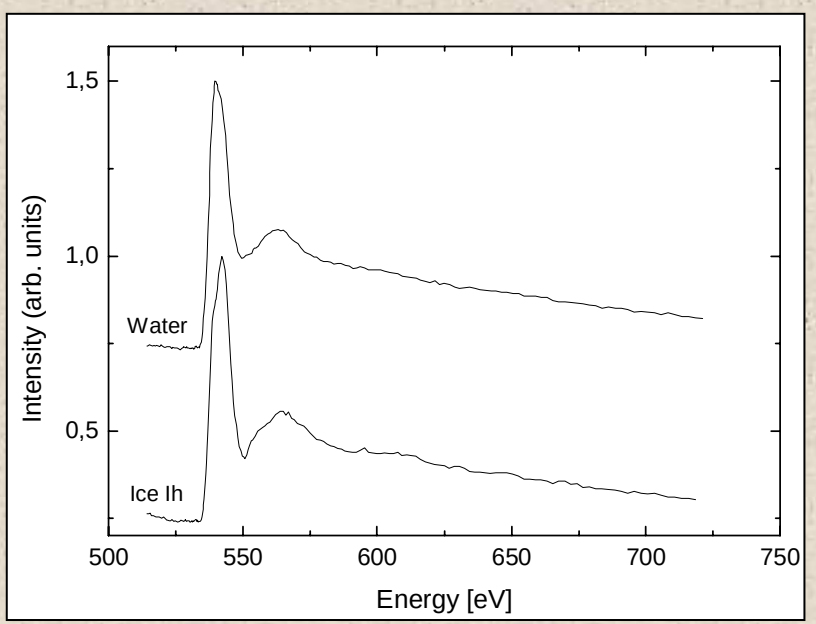

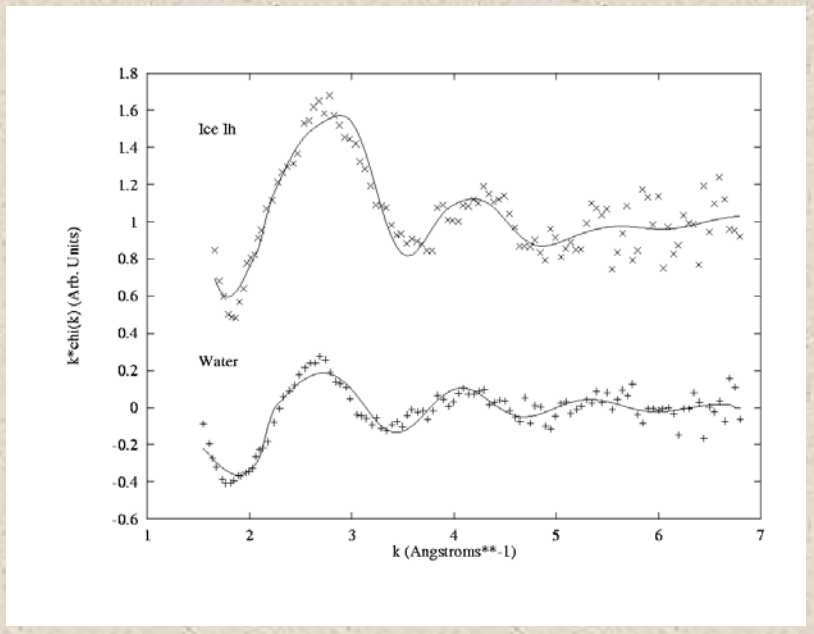

O-O partial radial distribution function

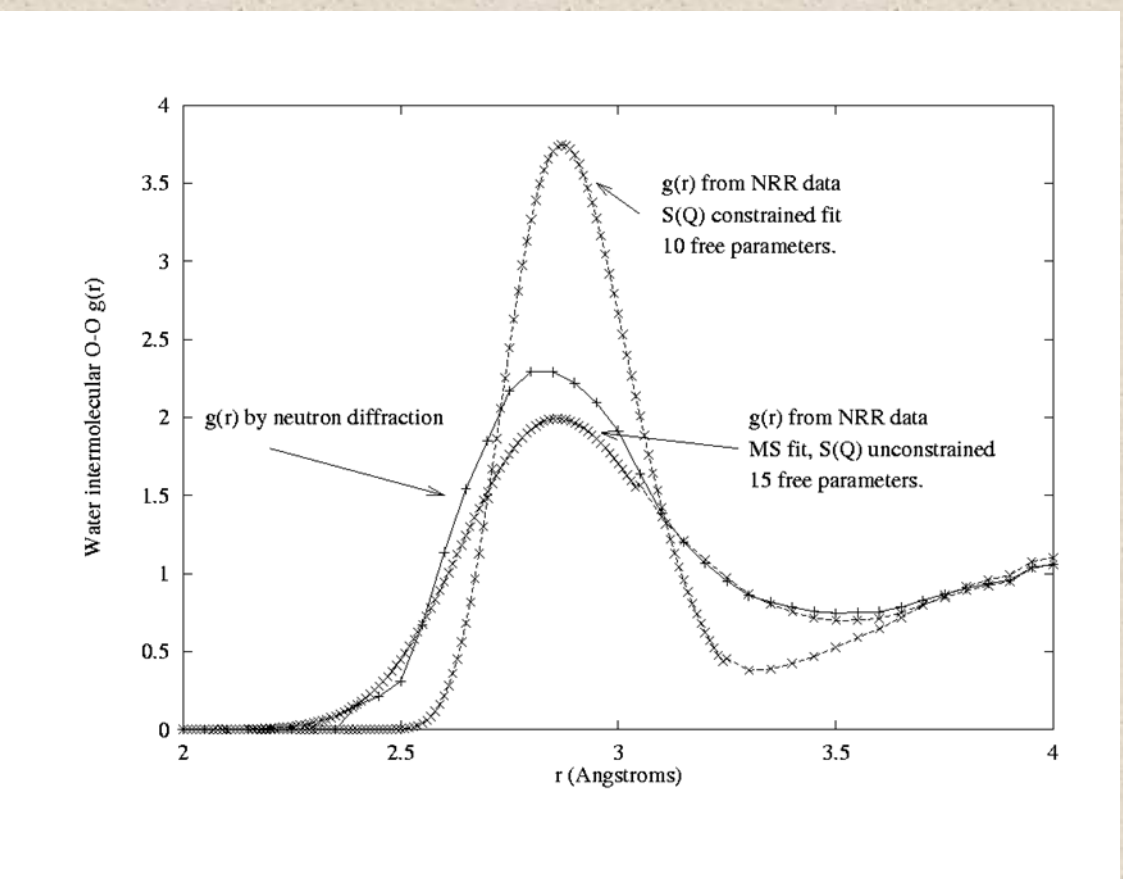

X-ray Raman Scattering:
O-O distance: 2.87 Å
Coordination: 4 - 7

Neutron Scattering:
O-O distance: 2.85 Å
Coordination: 4.4

XANES of the Oxygen K-edge in water

U. Bergmann et al.; Phys. Rev. B 66, 092107 (2002)

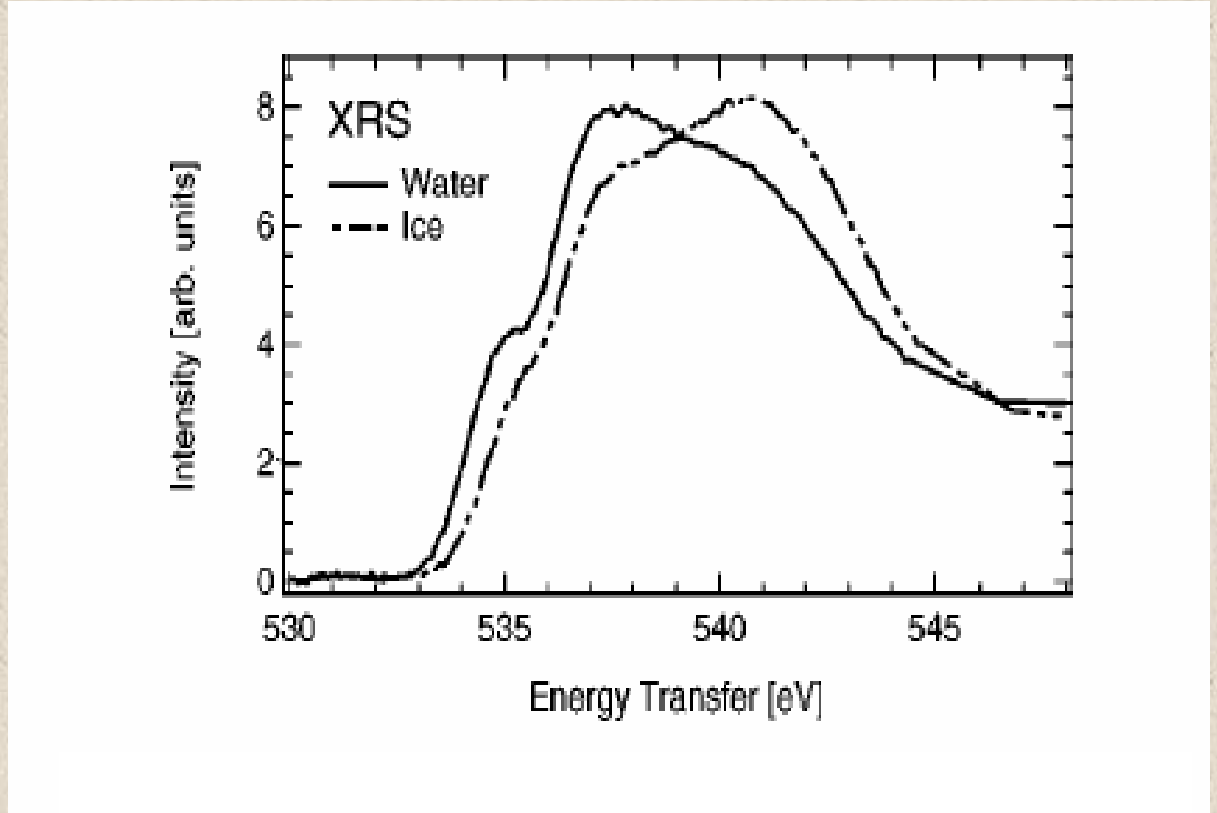

- XANES sensitive to the number of hydrogen bonds.
- Support by calculations.
- Analysis suggest significantly less than 3.5 H-bonds/molecule.

O K-edge XRS of the high-pressure phases of ice

Y.Q. Cai et al.; Phys. Rev. Lett. 94, 025502 (2005)

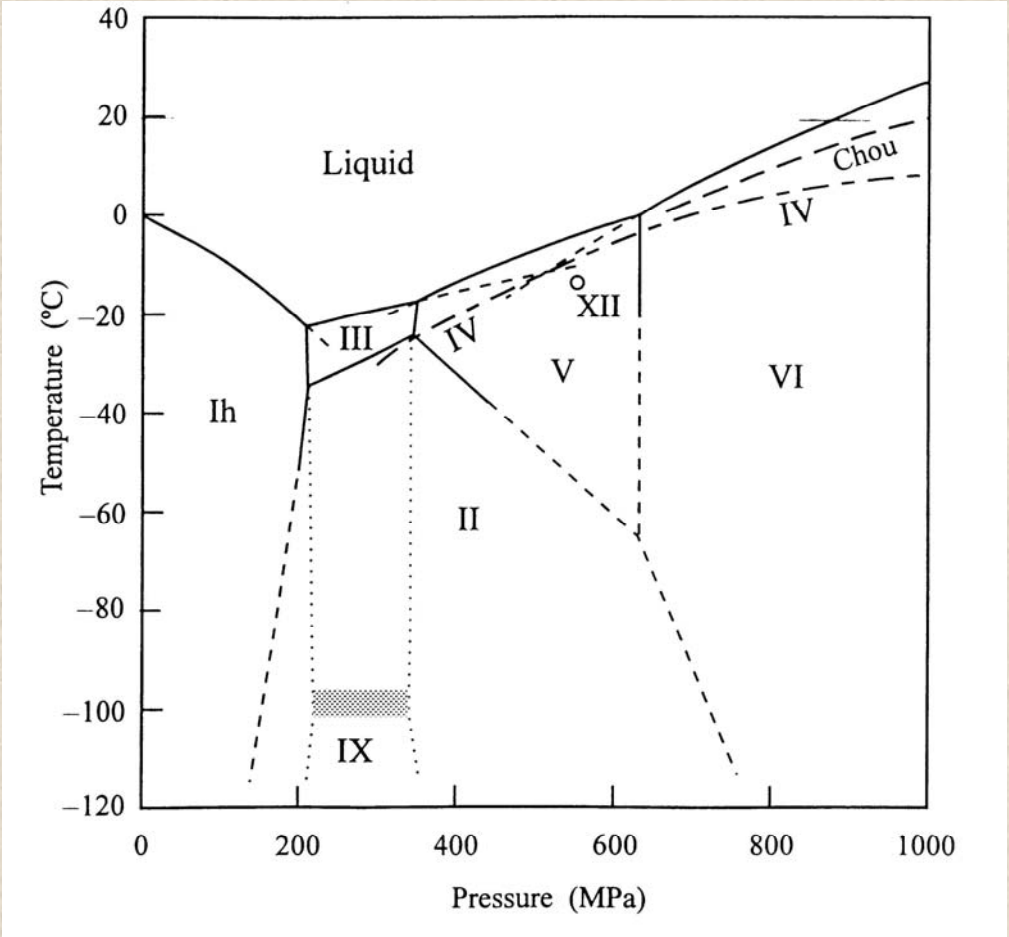

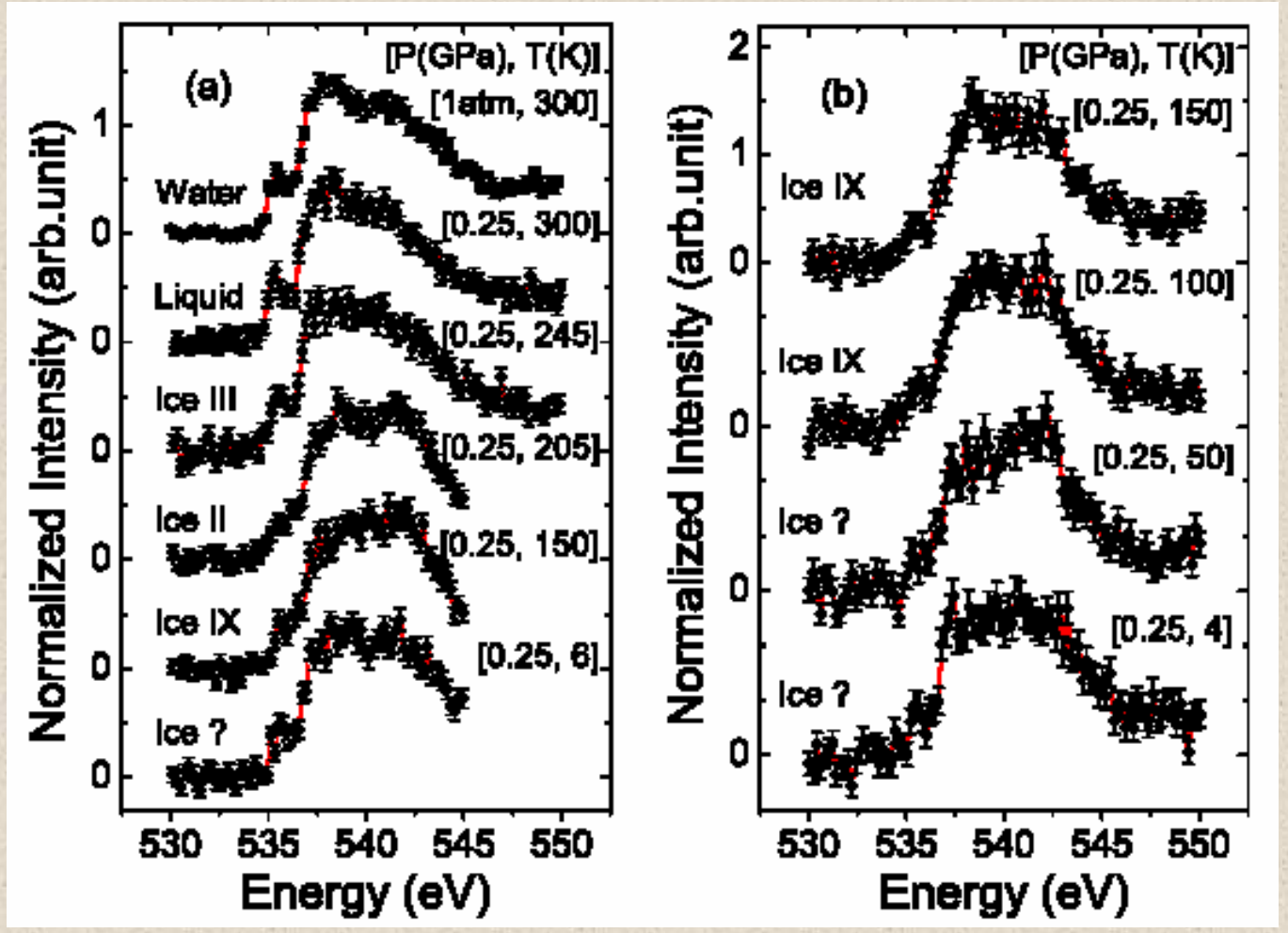

- Observation of spectral changes.
- Need of much better statistics and theory to extract quantitative information.

SUMMARY

Soft x-ray spectroscopy in the hard x-ray regime

- "simple" sample environment
- bulk sensitive
- access "exotic" final states
- extreme conditions: high temperature, high pressure

Weak probe

- practically limited to $Z < 14$
- limited quality for structural analysis (EXAFS)
- reasonable quality in the XANES region
- for high T, P measurements: cell window contribution critical

Exploit information contained in the near-edge region.

Resonant inelastic x-ray scattering

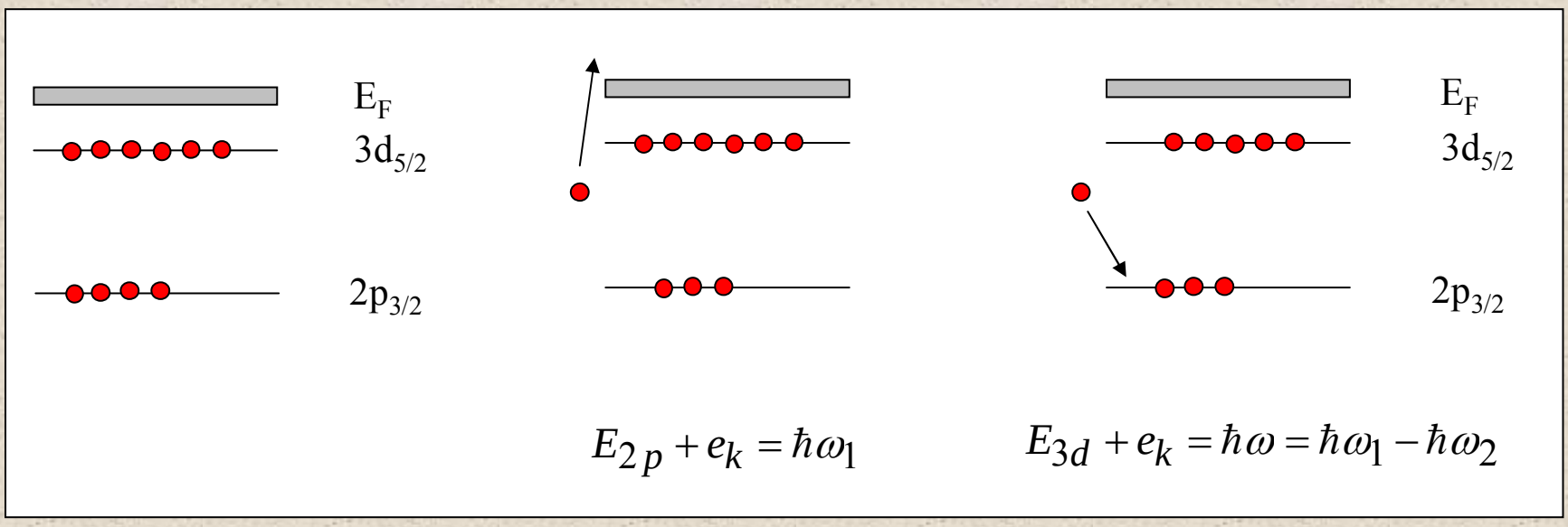

Emission Absorption

$$\frac{d^2\sigma}{d\hbar\omega_2 d\Omega} \approx \sum_f \left| \sum_n \frac{\langle f | C_{q'}^{(m)} | n \rangle \langle n | C_q^{(m)} | i \rangle}{E_i - E_f + \hbar\omega_1 - i\Gamma_n} \right|^2 \delta\left(E_f - E_i - \hbar\omega\right)$$

Resonant denominator

Resonant inelastic x-ray scattering at the L-edges of rare-earth materials

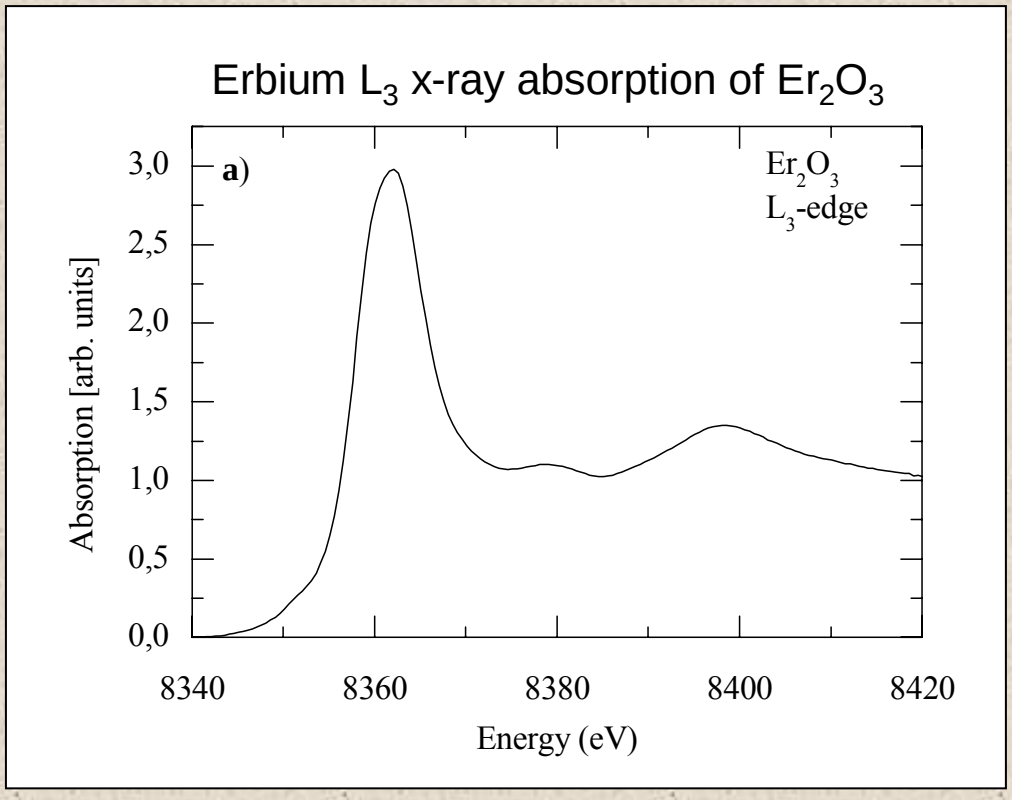

- Energy resolution is limited by the final state core-hole life time.

- Γ_L = 3 - 7 eV for the Rare-Earth elements.
  => additional absorption channels (if existing) might be obscured.

Resonant Inelastic X-ray Scattering

Er L_3 ($2p_{3/2}$) edge

decay channel:
$3d_{5/2} \rightarrow 2p_{3/2}$

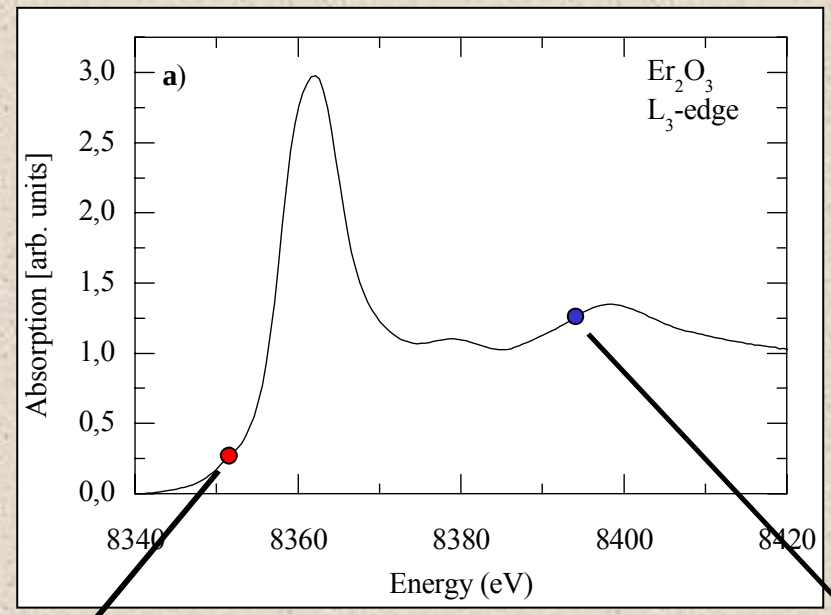

Spectral resolution limited by Γ_{2p}

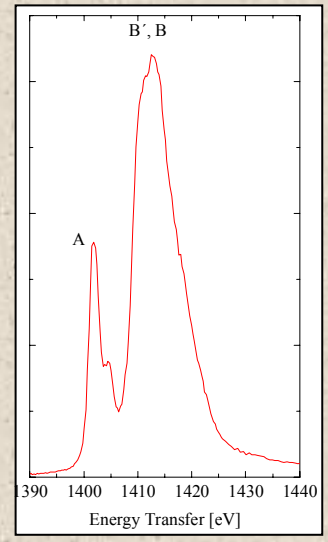

Spectral resolution limited by Γ_{3d}

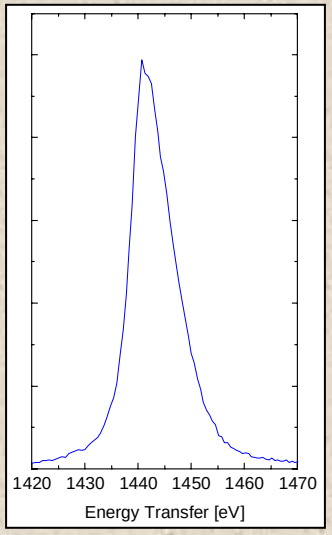

RIXS spectra at fixed incident energies around the absorption edge, monitoring the radiative $3d_{5/2}$ -> $2p_{3/2}$ decay channel.

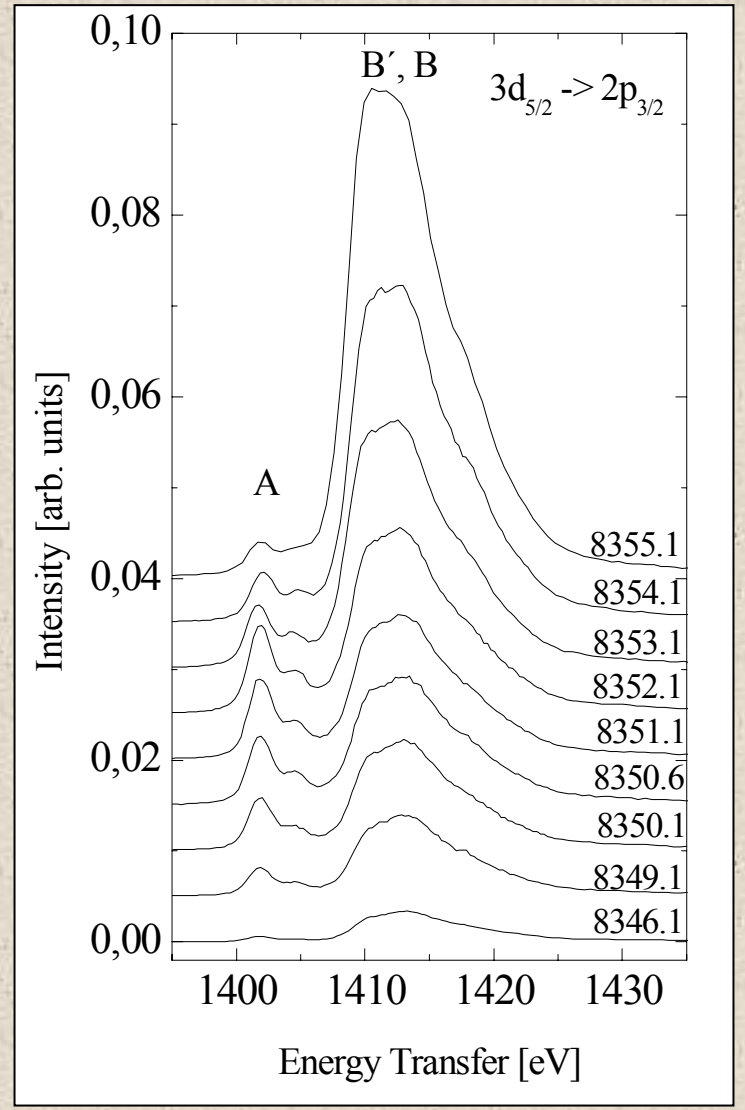

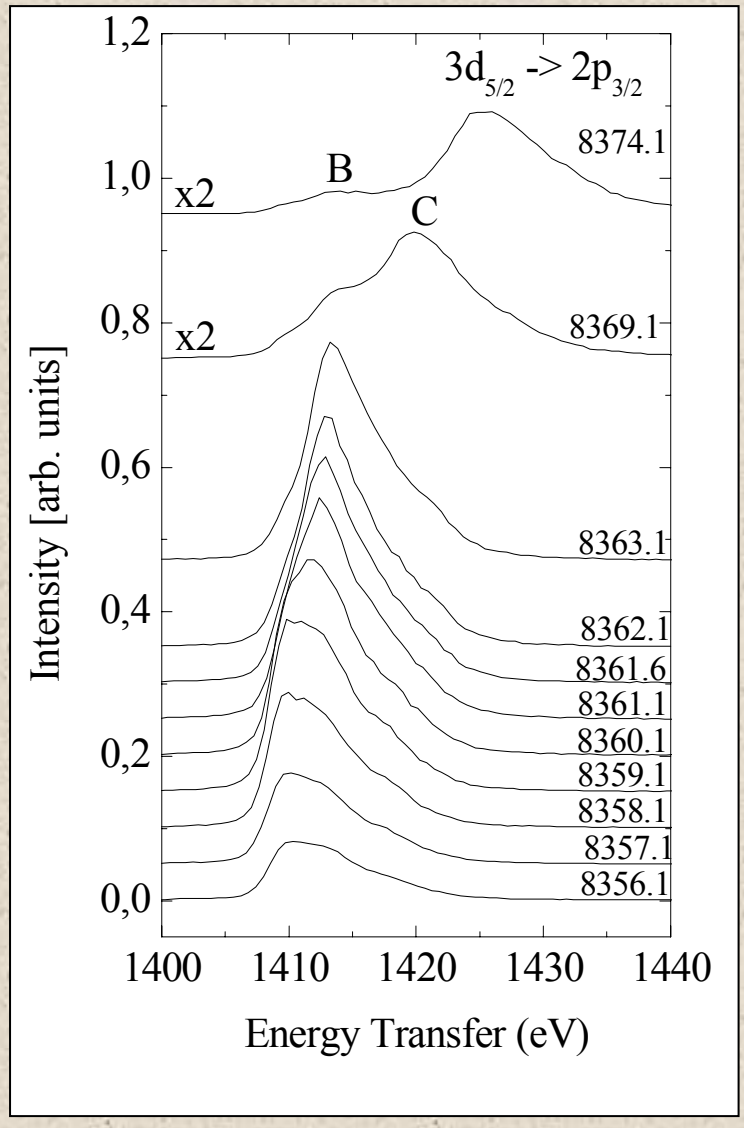

Observation of three different final state multiplet families:

A: very weak, only visible in the pre-edge region, always observed at constant energy transfer.
B: strong, always observed at constant energy transfer.
C: cannot be separated in pre-edge region, above edge observed at increasing energy transfer

Ground state of Er^{3+}: $|I\rangle = |4f^{11}5d^{0}\rangle$

$|F\rangle_c$: $|3d^{9}4f^{11}5d^{0}e_k\rangle$ <= $|N\rangle_c$: $|2p^{5}4f^{11}5d^{0}e_k\rangle$
(E1 excitation into continuum states and observation of $L\alpha_1$ fluorescence)

$|F\rangle_B$: $|3d^{9}4f^{11}5d^{1}\rangle$ <= $|N\rangle_B$: $|2p^{5}4f^{11}5d^{1}\rangle$
(E1 excitation into empty 5d states)

$|F\rangle_A$: $|3d^{9}4f^{12}5d^{0}\rangle$ <= $|N\rangle_A$: $|2p^{5}4f^{12}5d^{0}\rangle$
(E2 excitation into empty 4f states)

Intensity evolution of multiplet families as a function of $h\omega_1$ and character of features within one multiplet family

=>

Constant final state scans: $E_F - E_I = h\omega_2 - h\omega_1 = \text{constant}$

Constant Final State Scans

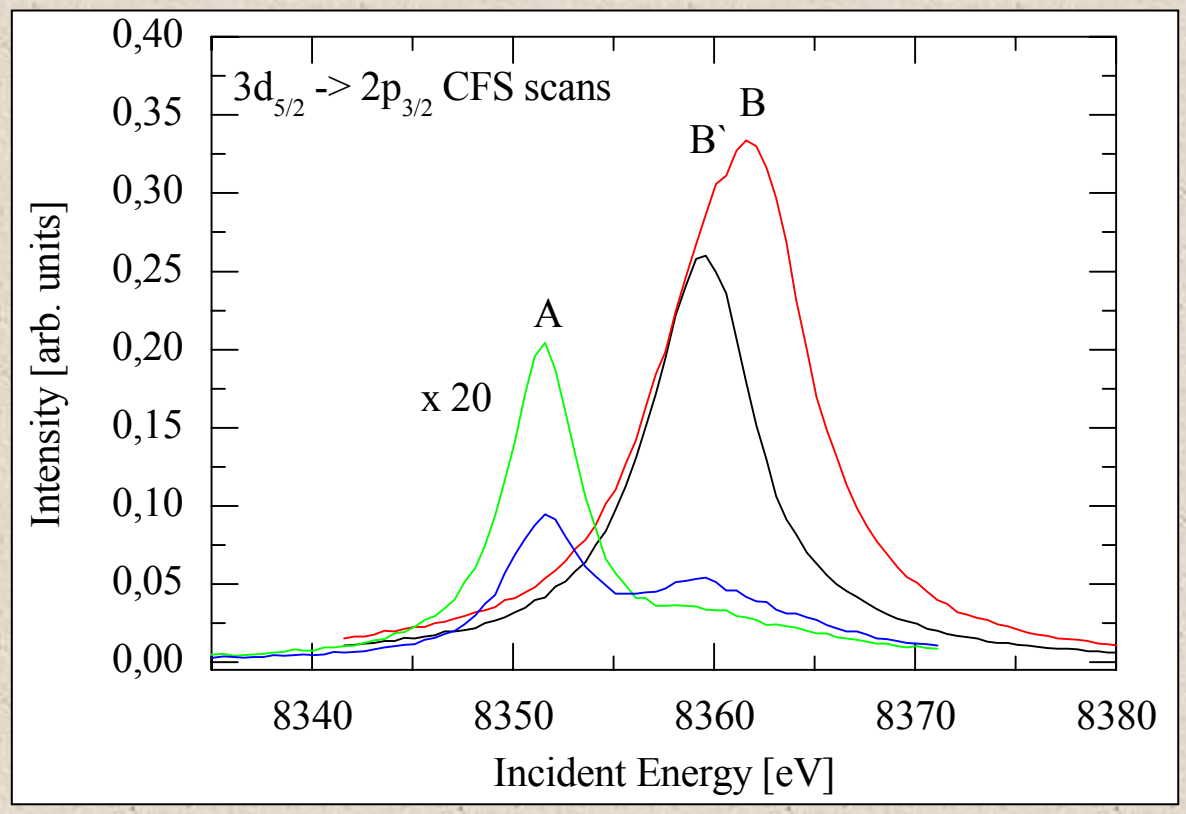

B and B*: 2p→5d dipolar transitions
different intermediate states, cubic field splitting of the 5d states: $\Delta E = 2.3$ eV

A and A*: 2p→4f quadrupolar transition
Same intermediate state, splitting due to spread of final state multiplet.

In summary:

RIXS allows the separation of different excitation channels which are obscured in a standard absorption measurement.

Condition:

Final state core-hole lifetime
<
energy separation of the multiplet families

RIXS at the L_3-edge of Yb in $YbInCu_4$ and $YbAgCu_4$

C. Dallera et al.; Phys. Rev. Lett. 88, 196403 (2002)

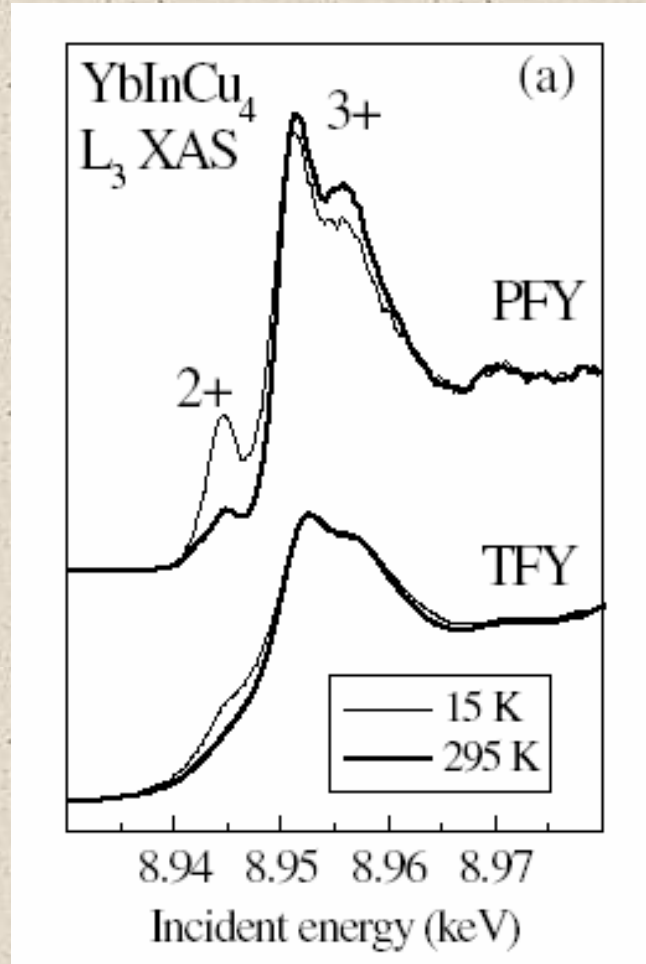

Mixed valence ground state

Yb^{3+}: $4f^{13}$

Yb^{2+}: $4f^{14}$

RIXS:
Enhancement of spectral contrast

Schematics of the RIXS 2p3d RIXS process

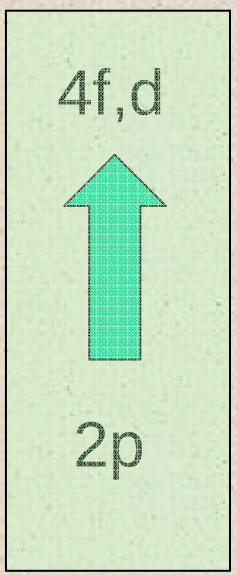

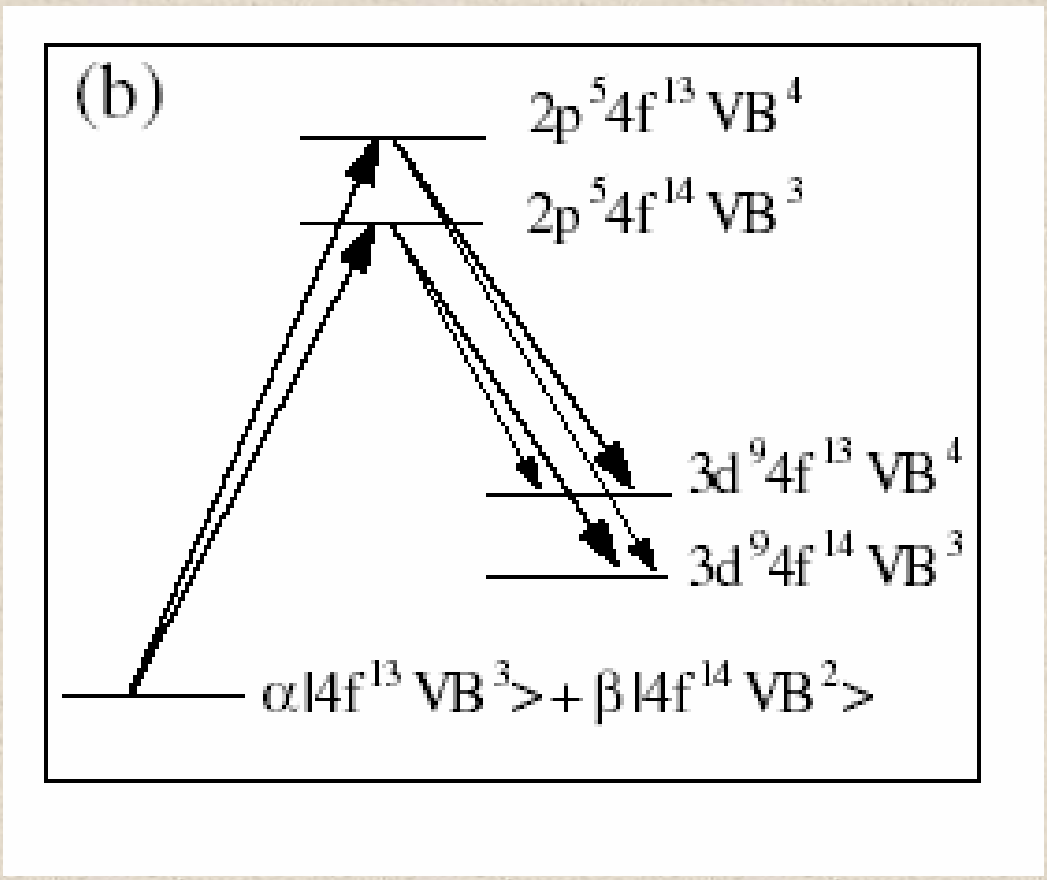

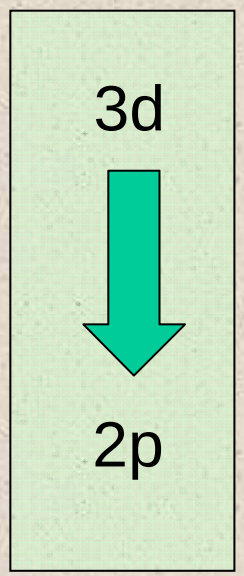

Dipolar excitations: $2p^6 4f^{13} VB^3 \rightarrow 2p^5 4f^{13} VB^4$

Quadrupolar excitations: $2p^6 4f^{13} VB^3 \rightarrow 2p^5 4f^{14} VB^3$

The resonant enhancement of the $2p^5 4f^{14}$ intermediate state

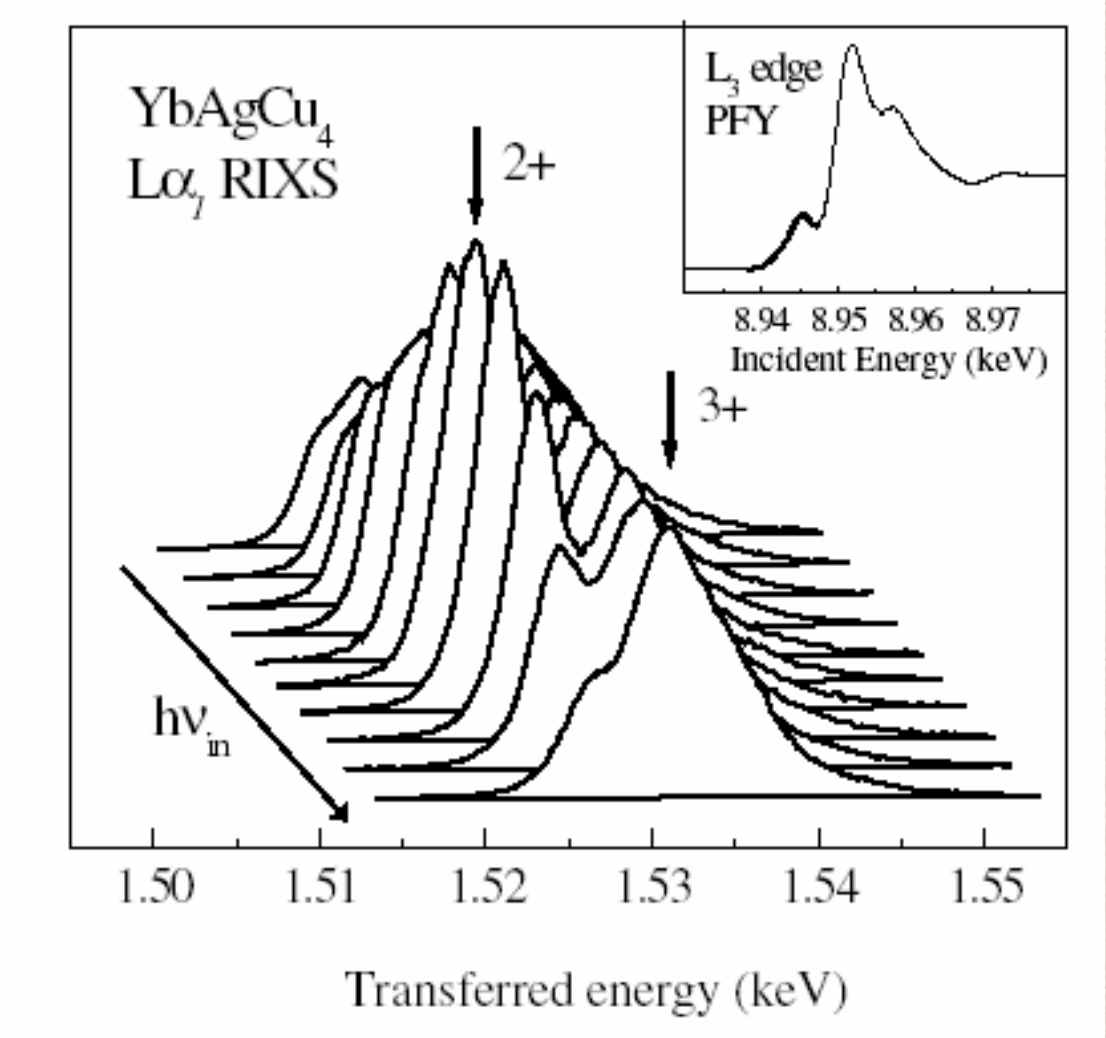

Temperature dependence of the $3d^9 4f^{14}$ final state multiplet

Sudden valence change

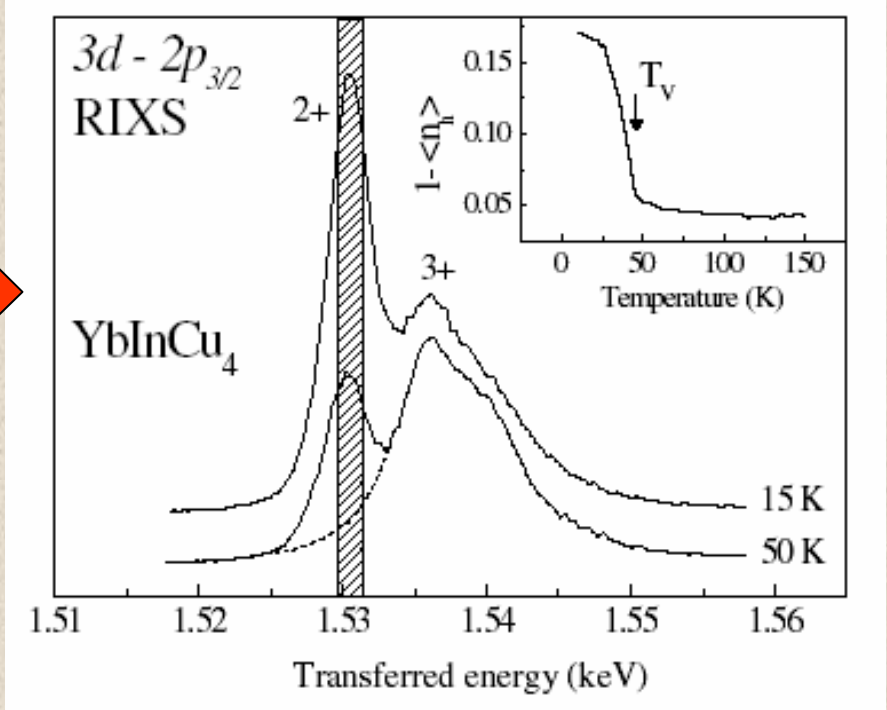

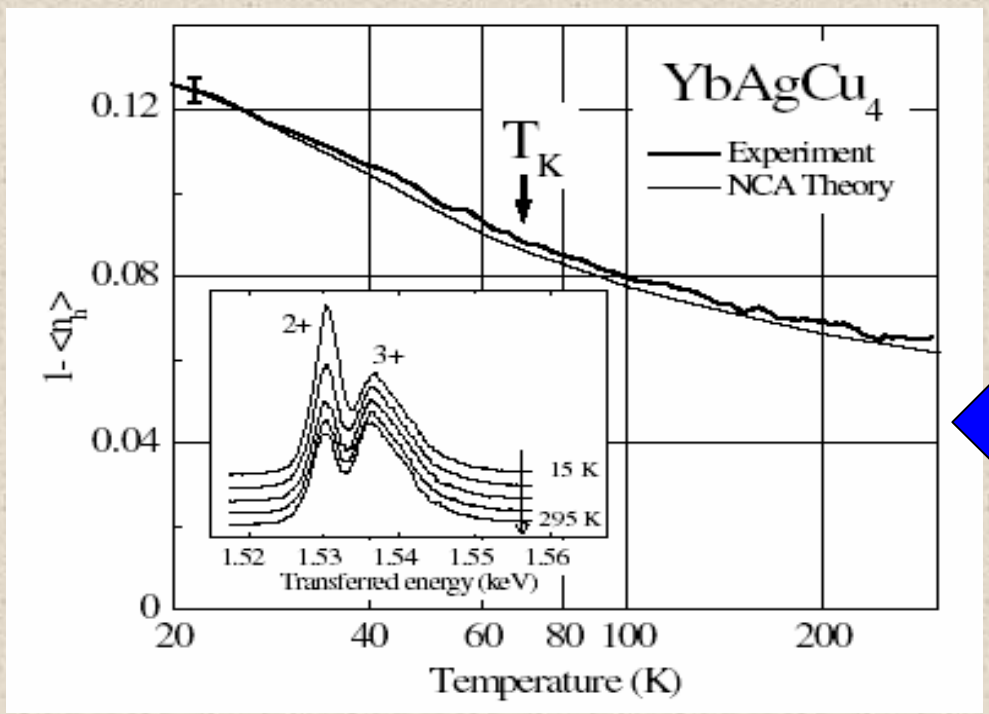

Smooth valence change

Partial Fluorescence Yield Absorption Spectroscopy

- Spectral sharpening by energy selection of radiative decay channel.
- E_{scatt} fixed, E_{inc} tuned through absorption edge.

Pt $L\beta_2$ emission line: $4d \rightarrow 2p_{3/2}$

Pt L_3-edge

$\Gamma_{L3} = 7$ eV

$\Gamma_{M4,5} = 1.9$ eV

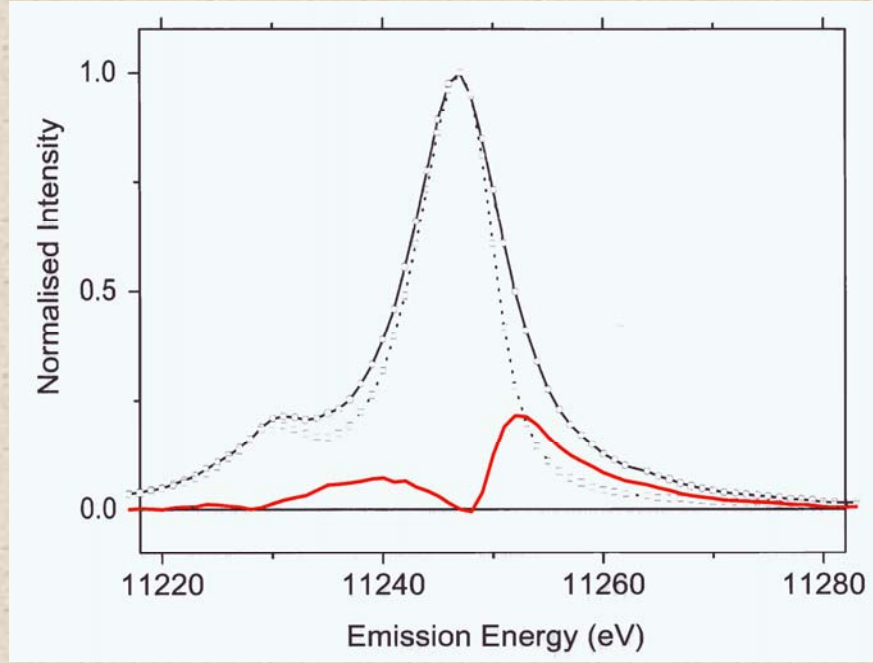

XAS L_3 edge of Pt metal

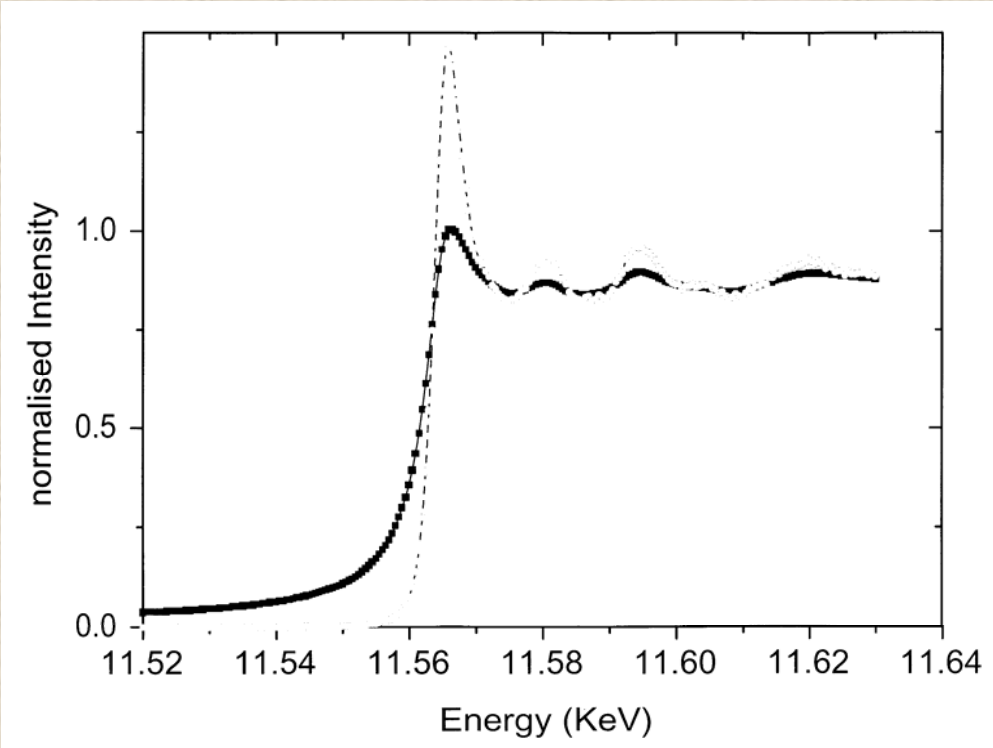

$$1/\Gamma_{PFY} = \sqrt{1/\Gamma_{2p}^2 + 1/\Gamma_{4d}^2}$$

Significant spectral sharpening !!!

High resolution X-ray Fluorescence

element

angular momentum

Fe 3p -> 1s radiative decay

valence (energy position)

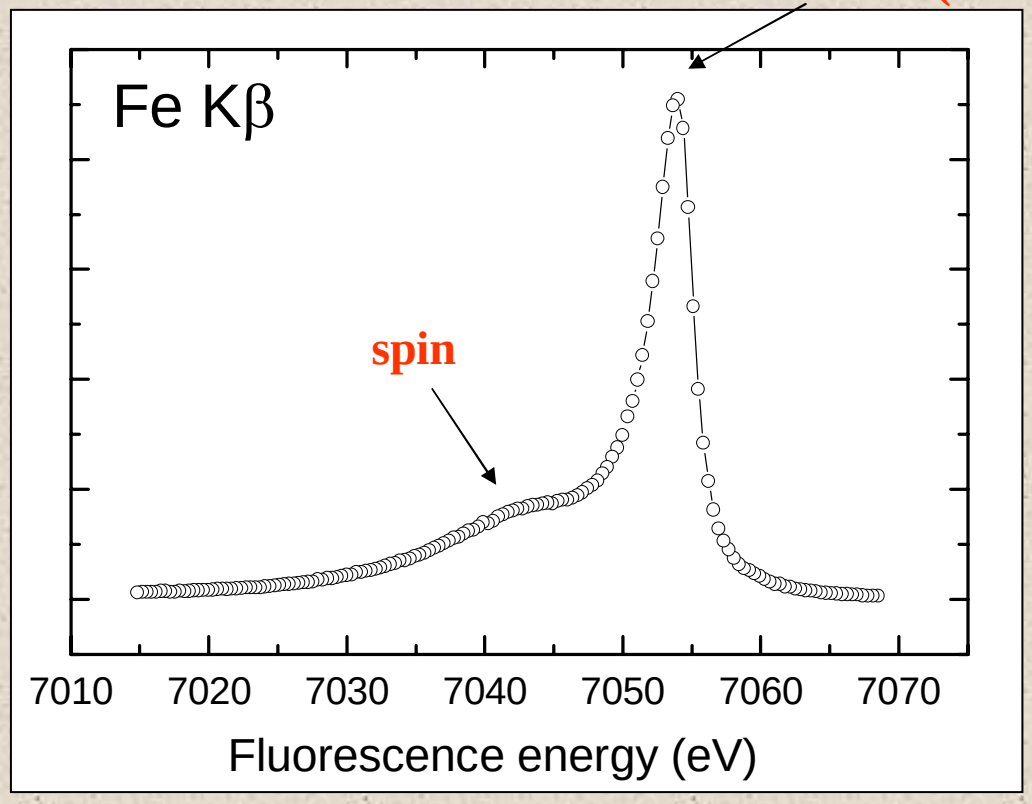

The pressure induced magnetic phase transition in iron metal.

Diamond Anvil cell

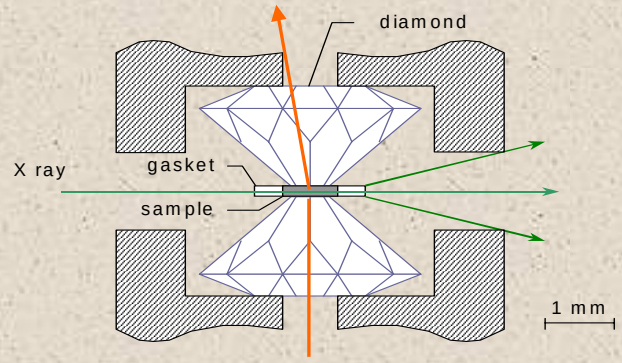

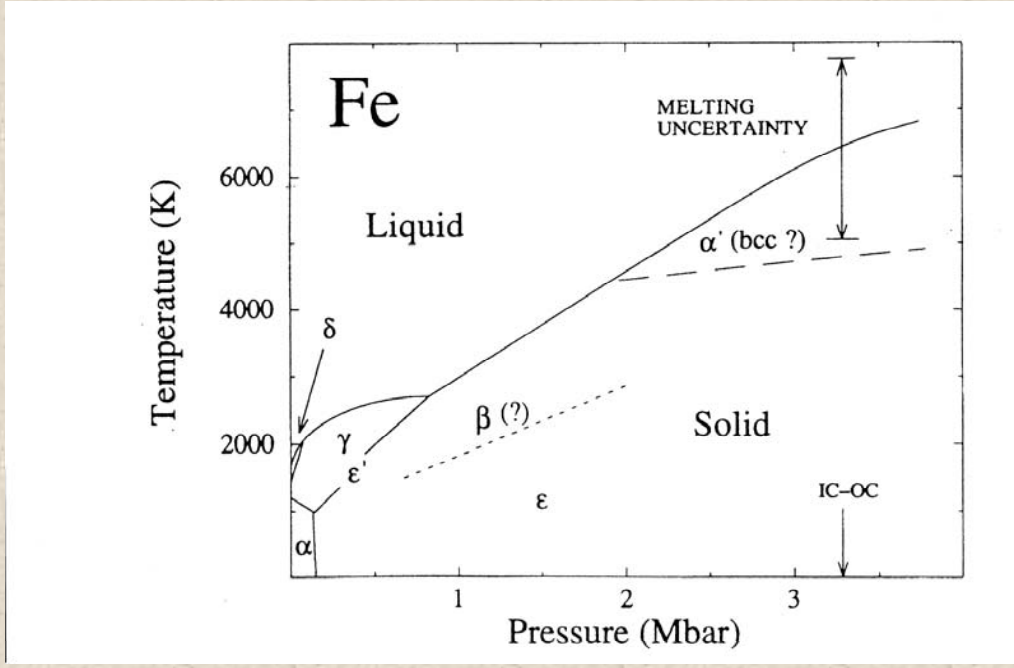

- small beam: 50-100 μm
- high flux
- X-ray diffraction as diagnostics tool

α (bcc) -> ε (hcp) at 13 GPa

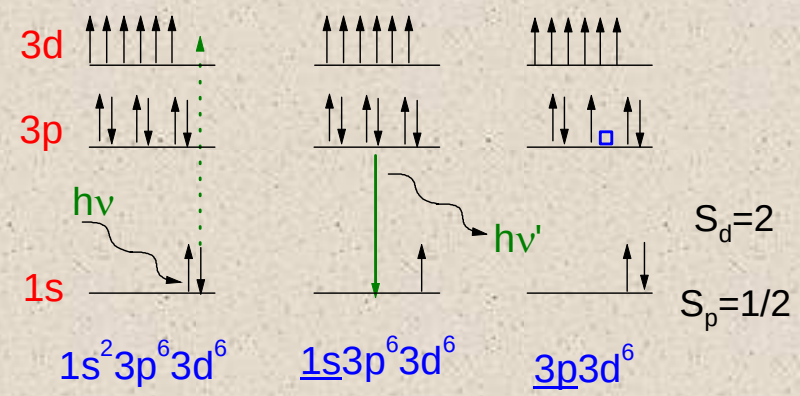

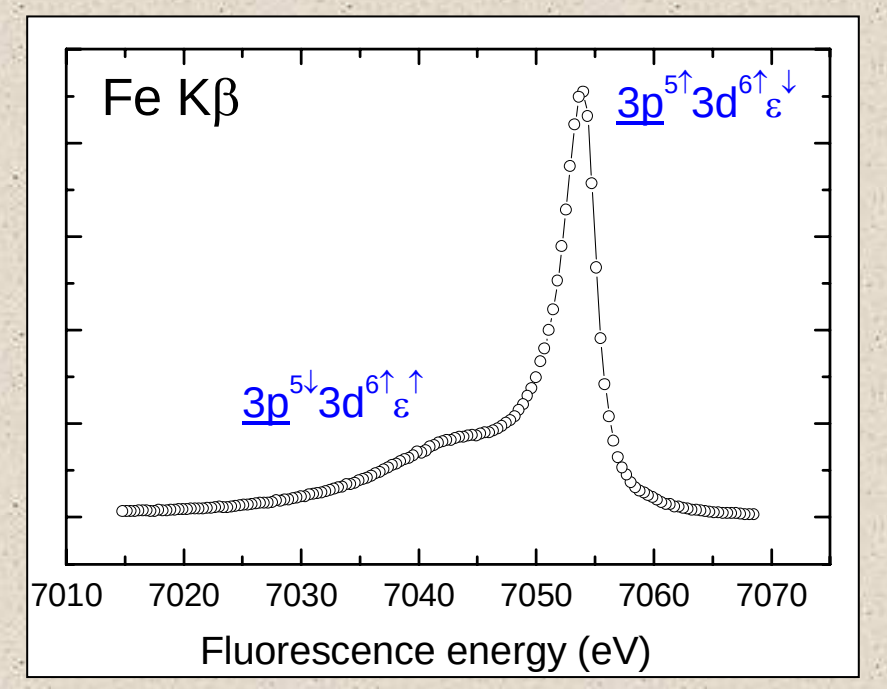

•Satellite structure arises from Coulomb- and exchange interactions between the 3p- and the 3d electrons.

• Main line: $S_d = 2$; $S_p = 1/2$, $e_{\downarrow}$ => spin-down character

• Satellite: $S_d=2$; $S_p= -1/2$, $e_{\uparrow}$ => spin-up character

Evidence magnetic phase transition through changes in emission line shape.

- intraatomic probe of the size of the 3d magnetic moment
- fast time scale: 10^{-15} s
- ferro-, antiferro-, ferri- and paramagnetic systems

Complementary to:

- X-ray magnetic circular dichroism (XMCD)
- Mössbauer spectroscopy

Fe Kβ emission spectra and Analysis

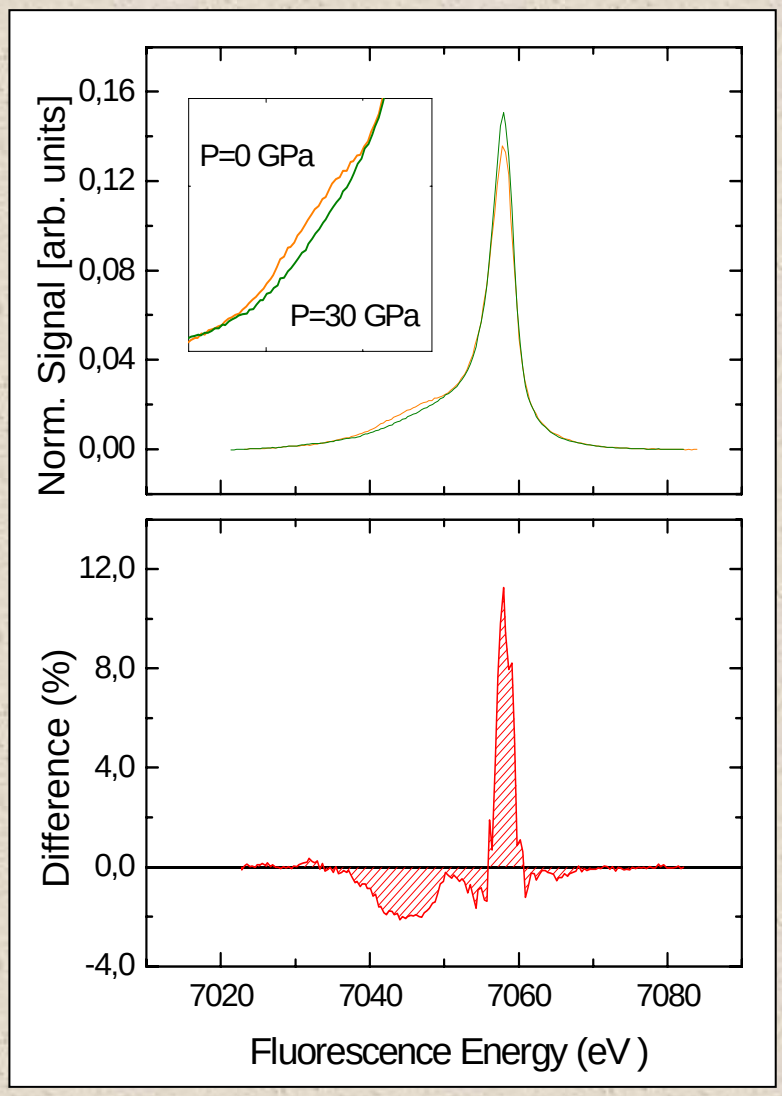

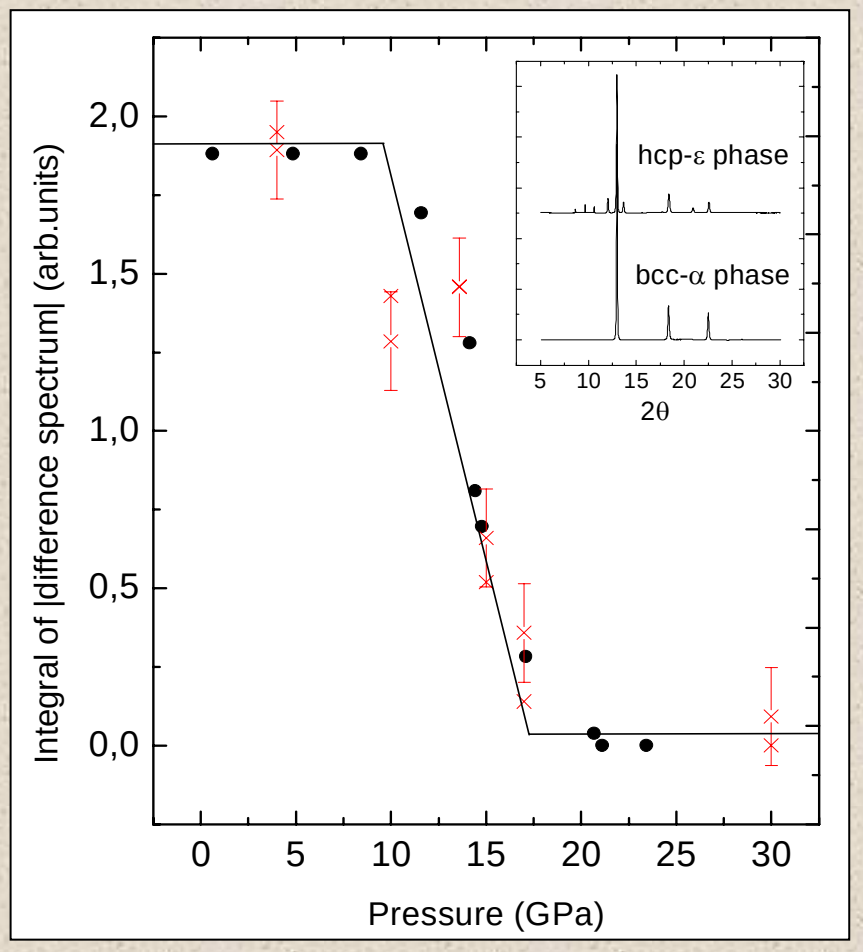

- Good agreement with Mössbauer and diffraction data.